WEDNESDAY 6 MAY 2015 – ROOM CAPRI

10.00-11.00 **SESSION 5: A FOCUS ON THE WORK-UP OF CUSHING'S SYNDROME: THE ROLE OF IMAGING**
Chairs: **Francesco Briganti, Sossio Cirillo**

10.00-10.15 THE IMAGING IN CUSHING'S DISEASE
Fabio Tortora

10.15-10.30 THE IMAGING IN ADRENAL CUSHING'S SYNDROME
Giovanni Vitale

10.30-10.45 THE IMAGING IN ECTOPIC CUSHING'S SYNDROME
Roberto Baldelli

10.45-11.00 Discussion and coffee break

Cushing's Syndrome

Rosario Pivonello, MD, PhD*,
Maria Cristina De Martino, MD, Monica De Leo,
Gaetano Lombardi, MD, Annamaria Colao, MD,

Endocrinol Metab Clin N Am
37 (2008) 135–149

ENDOCRINOLOGY AND METABOLISM CLINICS OF NORTH AMERICA

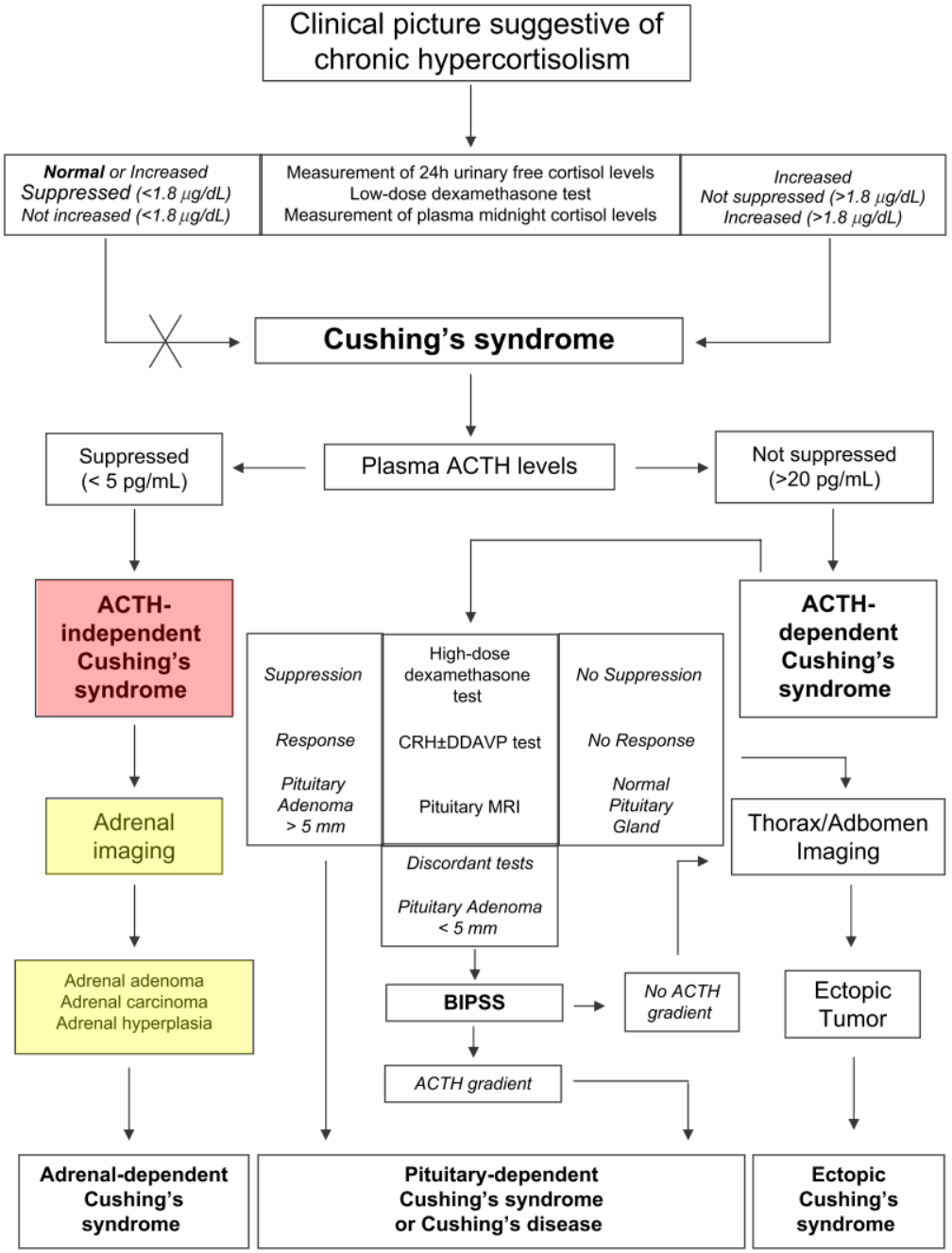

Fig. 1. Schematic procedure for the diagnosis and differential diagnosis of Cushing's syndrome.

Table 2 Clinical, biochemical and radiological features of adrenal Cushing

			Primary adrenocortical hyperplasia			
			Macronodular hyperplasia		Micronodular hyperplasia	
	Adrenocortical adenoma	Adrenocortical carcinoma	BMAH	c-BMAH	PPNAD	MAD
Frequency	~55%	~35%	Estimated 10%			
Age	All ages	All ages; familial cases in childhood	Fifth to sixth decade	Early childhood	Childhood or early adulthood	
Clinical presentation	Mild-to-severe Cushing	Moderate-to-severe Cushing with rapid onset and possible virilisation	Mild Cushing with insidious onset	Moderate-to-severe Cushing	Moderate-to-severe Cushing	
Biochemical features	Negative Liddle's test	Negative Liddle's test	Negative Liddle's test	Negative Liddle's test	Paradoxical cortisol response in Liddle's test	Negative Liddle's test
Radiological features	Solitary mass, often <4 cm, defined margins, homogeneous, <10 HFU, absolute washout >60%	Solitary mass, often >4 cm, irregular margins, heterogenous, >10 HFU, absolute washout <60%	Marked bilateral adrenal enlargement with multiple large non-pigmented nodules (1–5 cm)		Normal or small size adrenal glands with occasional small nodules (<1 cm)	

BMAH, primary bilateral macronodular adrenocortical hyperplasia; c-BMAH, childhood B HFU, Hounsfield unit; MAD, non-pigmented micronodular adrenocortical disease; PPNAD, primary pigmented nodular adrenocortical disease.

CT and MR Imaging of the Adrenal Glands in Cortisol-secreting Tumors*

ANTICANCER RESEARCH *31*: 2923-2926 (2011)

FRANCO LUMACHI[1], PAOLO MARCHESI[2], DIEGO MIOTTO[3] and RAFFAELLA MOTTA[3]

Computed Tomography Scanning

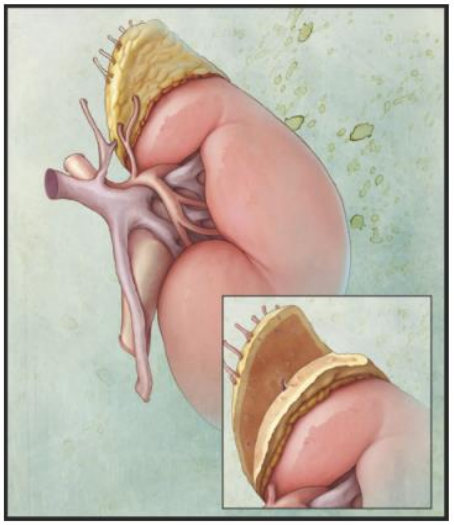

Figure 1. Drawing shows the normal adrenal gland.

In clinical practice, the adrenal glands can be well demonstrated with both single and multidetector CT scanners, using slice thickness 2.5-3 mm with 1.5-3 mm interval, before and after 100-150 ml of iodinated contrast administration. Usually, a portal venous phase (60-90 s) is preferred (8). Multidetector scanners offer higher performance, with collimation even smaller than 1 mm, allowing better multiplanar reconstructions (in coronal and sagittal planes), useful for depicting all anatomic relationships of the adrenal mass (9). On CT scan, normal adrenal glands appear symmetric and homogeneous, with a density approximately equal to that of the kidney (10).

J Clin Endocrinol Metab, July 2011, 96(7):2004–2015

Martha A. Zeiger, Stanley S. Siegelman, and Amir H. Hamrahian

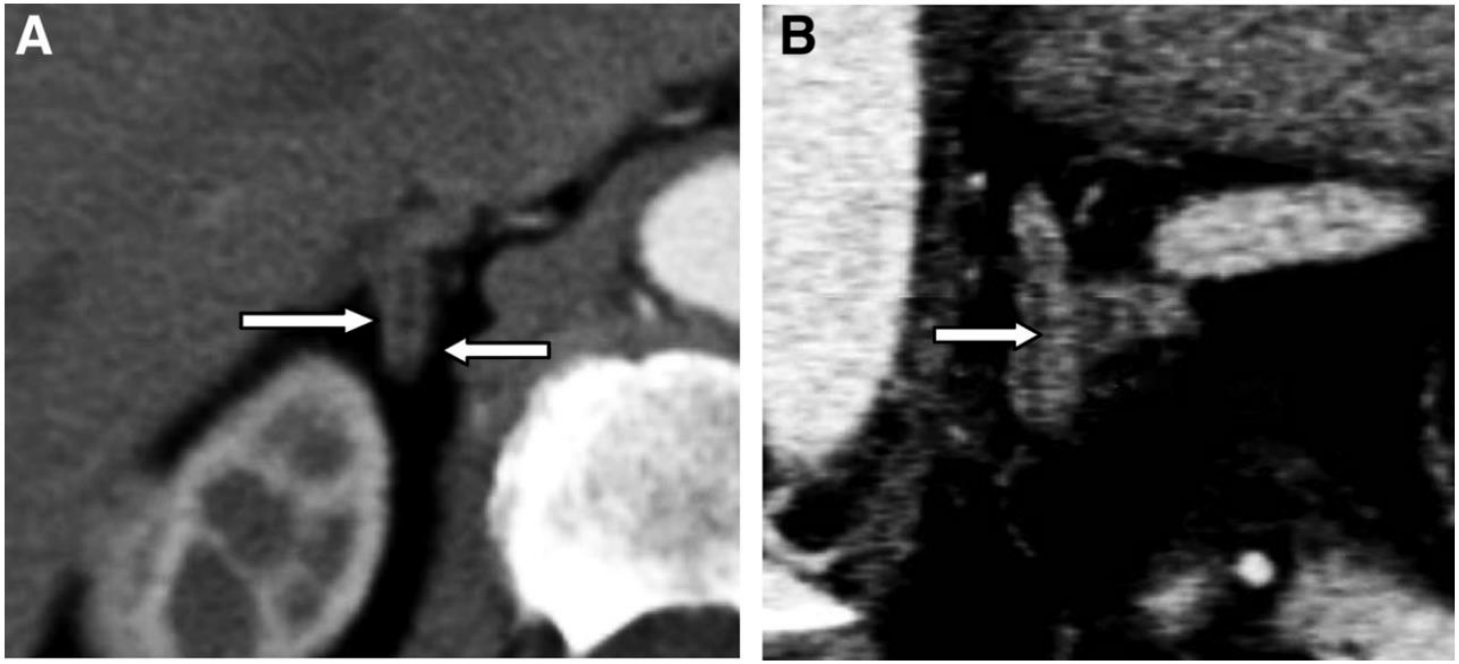

FIG. 1. A, Enhanced CT of normal right adrenal gland to illustrate distinction between adrenal cortex and medulla. The outer two layers of cortex enhance more avidly than the central layer of the medulla, revealing the "sandwich-like" nature of normal adrenal limbs. B, Enhanced CT of left adrenal gland in a different patient. The outer layers of cortex enhance to a greater degree than the centrally located adrenal medulla.

CT and MR Imaging of the Adrenal Glands in Cortisol-secreting Tumors*

ANTICANCER RESEARCH *31*: 2923-2926 (2011)

FRANCO LUMACHI[1], PAOLO MARCHESI[2], DIEGO MIOTTO[3] and RAFFAELLA MOTTA[3]

Adrenal adenomas usually appear relatively small (1-5 cm), round or ovoid, homogeneous, with smooth borders and lower than water density (<10 Hounsfield units [HU] without contrast), due to abundant intracellular lipid content (9-13). Two thirds of adenomas contain significant intracellular lipid and show the typical unenhanced CT attenuation <10 HU, while 25-30% of them are lipid-poor, with unenhanced CT attenuation >10 HU (10, 14, 15).

Adrenal neoplasms

G. Low [a,*], H. Dhliwayo [a], D.J. Lomas [b]

Clinical Radiology 67 (2012) 988–1000

- **Fat approximately -30 to -100 HU**
- **A 10 HU unenhanced CT threshold had 71% sensitivity and 98% specificity in diagnosing adenomas**

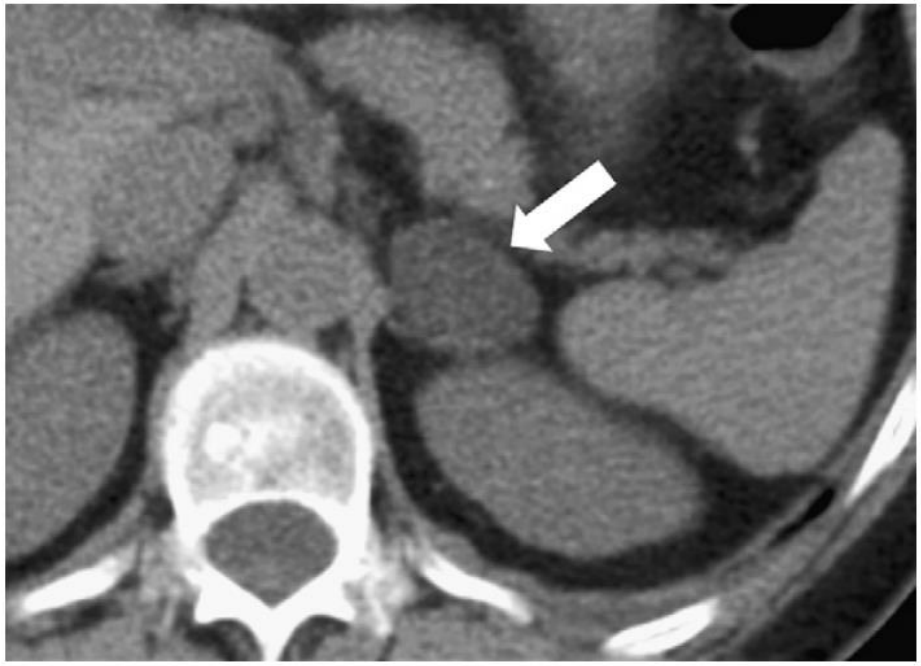

Figure 1 Axial, unenhanced CT image shows a lipid-rich left adrenal adenoma (arrow). The small, ovoid-shaped, well-defined tumour has a homogeneous low attenuation of approximately −0.7 HU.

Lipid-Poor Adenomas on Unenhanced CT: Does Histogram Analysis Increase Sensitivity Compared with a Mean Attenuation Threshold?

Lisa M. Ho[1]
Erik K. Paulson[1]
Matthew J. Brady[1]
Terence Z. Wong[1]
Sebastian T. Schindera[1,2]

AJR 2008; 191:234–238

Fig. 1—68-year-old woman with right adrenal adenoma.
A, Unenhanced CT scan shows region of interest (ROI) placed on lesion. Mean attenuation is –5.4 H.
B, CT histogram analysis shows that for this ROI, 92 pixels measure less than 0 H. Total of 135 pixels results in 68% negative pixels calculated for this adrenal adenoma.

A

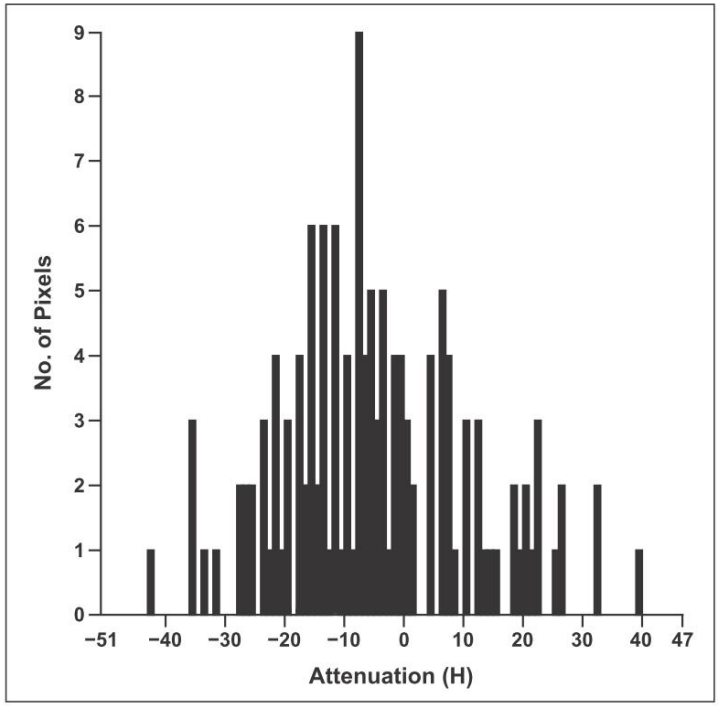

B

TABLE 2: Sensitivity and Specificity for Diagnosis of Adenomas Using Thresholds of > 5% Negative Pixels, > 10% Negative Pixels, and 10-H Mean CT Attenuation

Threshold	Sensitivity (%)	95% CI	Specificity (%)	95% CI
Negative pixels, 5%	90	(81–95)	94	(80–99)
Negative pixels, 10%	84	(77–92)	100	(92–100)
Mean CT attenuation, ≤ 10 H	68	(58–78)	100	(92–100)

RadioGraphics September-October 2009

Pamela T. Johnson, MD • Karen M. Horton, MD • Elliot K. Fishman, MD

Figure 3. Drawing shows the enhancement pattern of a lipid-poor adenoma.

CT and MR Imaging of the Adrenal Glands in Cortisol-secreting Tumors*

ANTICANCER RESEARCH *31*: 2923-2926 (2011)

FRANCO LUMACHI[1], PAOLO MARCHESI[2], DIEGO MIOTTO[3] and RAFFAELLA MOTTA[3]

Large adenomas may appear inhomogeneous, containing cystic degeneration, calcifications, hemorrhage and necrosis (15). On contrast-enhanced CT, performed 60 s and 15 min after intravenous contrast medium administration, adenomas show both a rapid enhancement and a rapid wash-out loss of contrast, while non-adenomas typically show a slower contrast washout phase (Figure 2). When the 15-min delay protocol is used, an absolute contrast wash-out of >60% and a relative contrast washout of >40% have 86-88% sensitivity and 92-98% specificity for the diagnosis of adenomas, respectively (9, 10, 12, 14). With the

Figure 2 Lipid-poor adenoma. (A) Unenhanced CT of the abdomen showing a right adrenal mass with a HU measurement of 15 HU (arrow). (B) Contrast-enhanced CT acquired 60 s after administration of i.v. contrast shows enhancement of the adrenal mass to 75 HU. (C) On delayed CT, acquired 15 min after administration of i.v. contrast, the mass measures 25 HU. These measurements provide an absolute contrast enhancement washout of 83% and a relative contrast washout of 67% proving a lipid-poor adenoma.

CT and MR Imaging of the Adrenal Glands in Cortisol-secreting Tumors*

ANTICANCER RESEARCH *31*: 2923-2926 (2011)

FRANCO LUMACHI[1], PAOLO MARCHESI[2], DIEGO MIOTTO[3] and RAFFAELLA MOTTA[3]

Magnetic Resonance Imaging

The appropriate MR imaging study protocol of adrenal glands should include (9): T1-weighted (T1w) gradient-recalled echo (GRE) sequences in- and out-of-phase, slice thickness of 3-5 mm; T2-weighted (T2w) turbo spin-echo (TSE) sequences with fat suppression, slice thickness of 3-5 mm and T2w half-Fourier acquisition single-shot turbo-spin-echo (HASTE) sequences, slice thickness of 5 mm. The use of breath-hold sequences mostly eliminates most motion artifacts (16). Intravenous gadolinium (Gd) administration allows the characterization of the vascular pattern of adrenal masses, like contrast-enhanced CT. Axial images are standard, while coronal and sagittal images may help in delineating large adrenal masses (9). On MR, normal adrenal glands show low to intermediate T1- and T2-signal intensity, equal to or slightly lower than that of the normal liver (11, 14). Adrenal adenomas usually appear

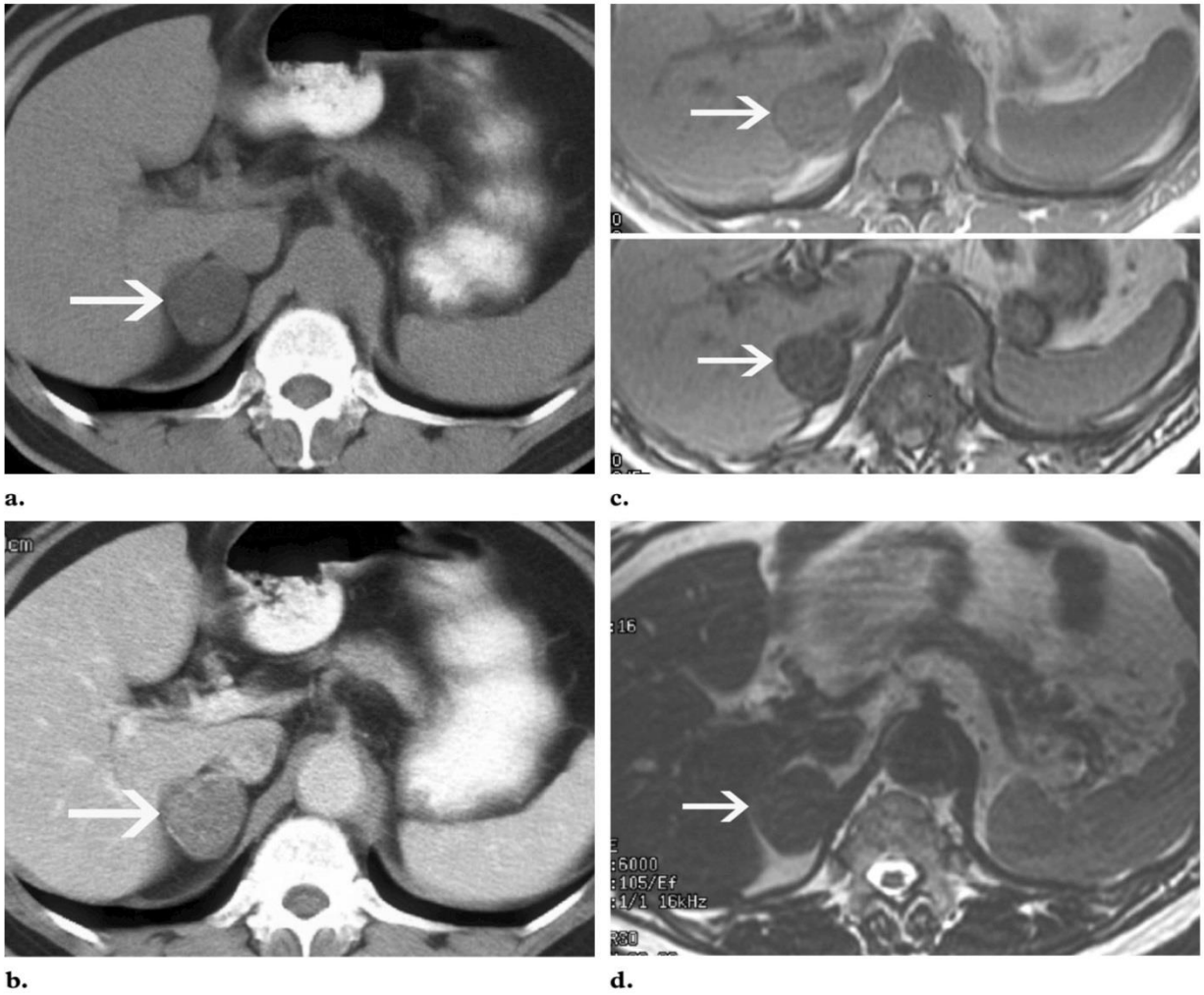

Chemical shift imaging is a lipid-sensitive MRI technique that exploits the resonance frequency differences of fat and water. Adenomas that possess significant intracytoplasmic fat show signal loss on the opposed-phase compared to the in-phase with 81–100% sensitivity and 94–100% specificity reported (Fig 2).[1] The percentage signal loss can be calculated using the adrenal signal intensity (SI) index, $[(SI_{\text{In phase}} - SI_{\text{Opposed phase}})/SI_{\text{In phase}} \times 100\%]$ with a value $\geq$16.5% considered diagnostic for an adenoma.[1] Provided

Figure 1. Adrenal adenoma in a 68-year-old man. **(a)** Unenhanced CT scan shows a smooth, ovoid, well-defined low-attenuation mass (arrow). The CT attenuation value was −5 HU, indicating the presence of intracellular lipid. Korobkin et al (8) demonstrated a cut-off point of 18 HU, below which an adrenal lesion may be designated as a benign adenoma with a specificity of 85% and a sensitivity of 100%. **(b)** Contrast material–enhanced CT scan shows moderate enhancement of the mass (arrow), which gives the lesion a slightly heterogeneous appearance. **(c)** Axial in-phase (repetition time msec/echo time msec = 150/4.2) (top) and out-of-phase (150/1.8) (bottom) fast multiplanar spoiled gradient-echo (FMPSPGR) T1-weighted MR images (flip angle = 90°) show the mass with classic signal dropout (arrow), a finding that suggests the presence of intracellular lipid, a characteristic feature of benign adenomas. **(d)** On an axial fast spin-echo T2-weighted MR image (6,000/105), the adenoma (arrow) is isointense relative to the liver. **(e)** High-power photomicrograph (original magnification, ×400; hematoxylin-eosin [H-E] stain) demonstrates a lipid-rich adrenal adenoma with abundant intracellular fat (arrow).

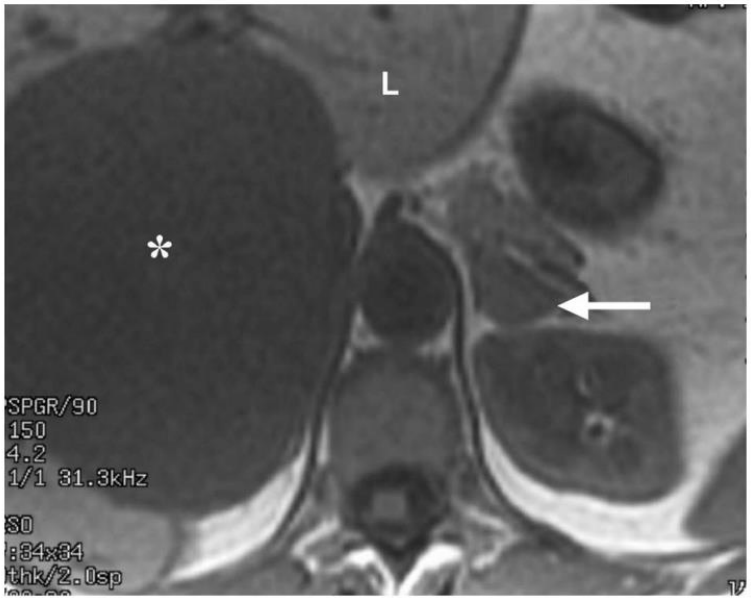

a.

b.

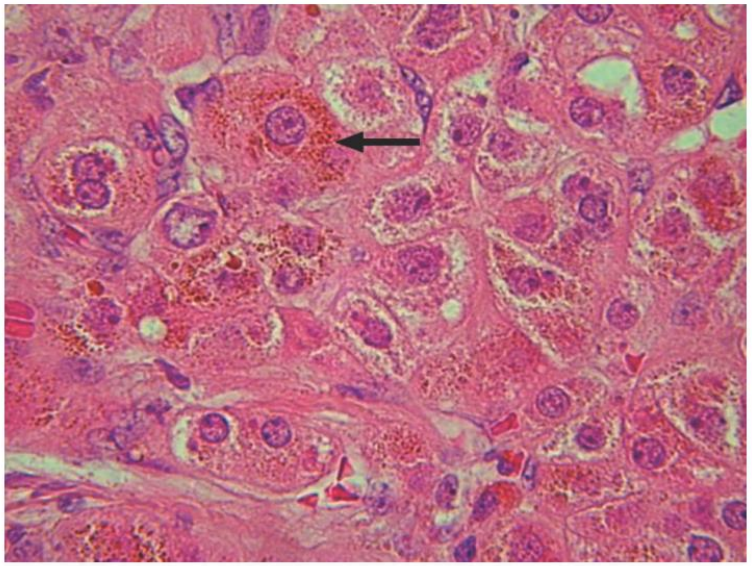

c.

Figure 2. Small adenoma in a 51-year-old woman. **(a)** Axial in-phase FMPSPGR T1-weighted MR image (150/4.2, flip angle = 90°) shows an ovoid mass that arises from the medial limb of the left adrenal gland (arrow). A large hemangioma (*) was seen incidentally in the liver *(L)*. **(b)** Axial out-of-phase FMPSPGR T1-weighted MR image (150/1.8, flip angle = 90°) shows no signal dropout in the mass (arrow). This finding is uncharacteristic of adenomas, which classically show signal dropout with the out-of-phase sequence. *L* = liver, * = hemangioma. **(c)** Photomicrograph (original magnification, ×400; H-E stain) shows a lipid-poor adrenal adenoma that contains predominantly eosinophilic compact cells with abundant lipofuscin pigment, which appears brown (arrow). These histologic findings may account for the lack of signal dropout in **b**.

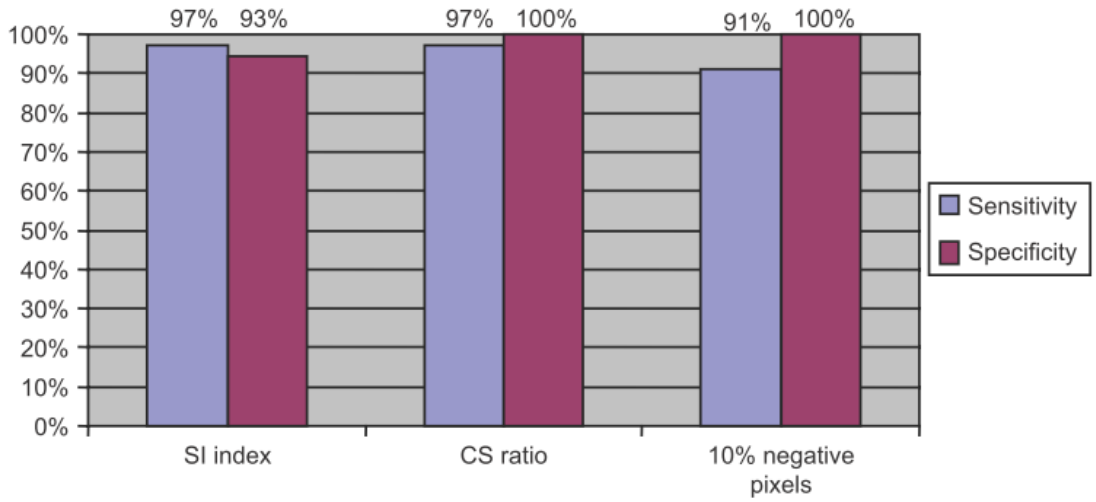

Fig. 4. Bar chart comparing sensitivity values of signal intensity (SI) index and chemical-shift (CS) ratio formulas of chemical-shift MRI to 10% negative pixel threshold of CT histogram analysis on unenhanced CT for adenoma diagnosis.

Conclusion: CT histogram analysis method using a 10% negative pixel threshold on unenhanced CT had a good sensitivity and perfect specificity for the differentiation of adrenal adenomas from non-adenomas. In spite of the good results obtained with the CT histogram analysis method, chemical-shift MRI using adrenal-to-spleen chemical-shift ratio and adrenal signal intensity index formulas had a higher sensitivity and could help in the characterization of adrenal masses appearing indeterminate by CT histogram analysis.

Adenoma *vs* Metastases

Characterization of Lipid-Poor Adrenal Adenoma: Chemical-Shift MRI and Washout CT

Jung Min Seo[1]
Byung Kwan Park
Sung Yoon Park
Chan Kyo Kim

AJR 2014; 202:1043–1050

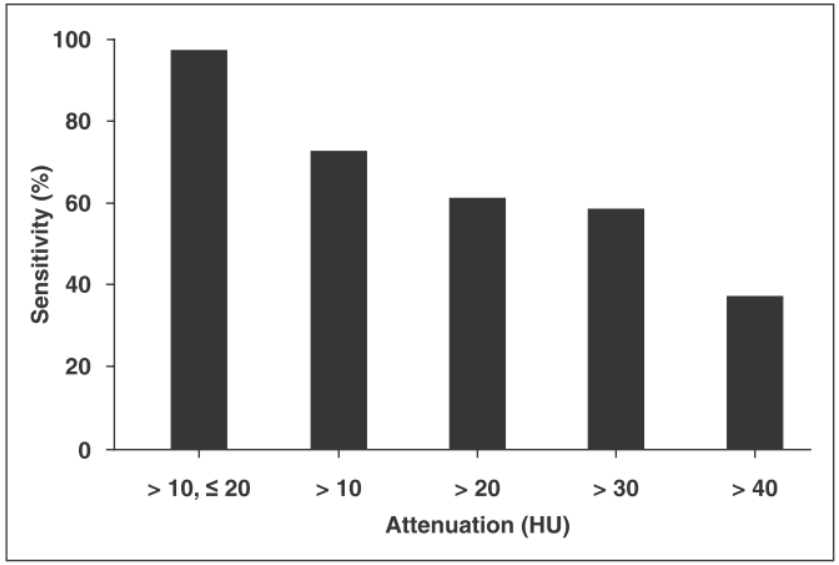

Fig. 2—Graph shows MRI sensitivity for lipid-poor adenomas. MRI sensitivity for lipid-poor adenomas measuring greater than 10 HU and 20 HU or less on unenhanced CT is 100% (12/12), whereas sensitivities for lipid-poor adenomas measuring greater than 20, greater than 30, and greater than 40 HU decreases to 64.0% (16/25), 61.5% (8/13), and 40% (2/5), respectively.

Small series

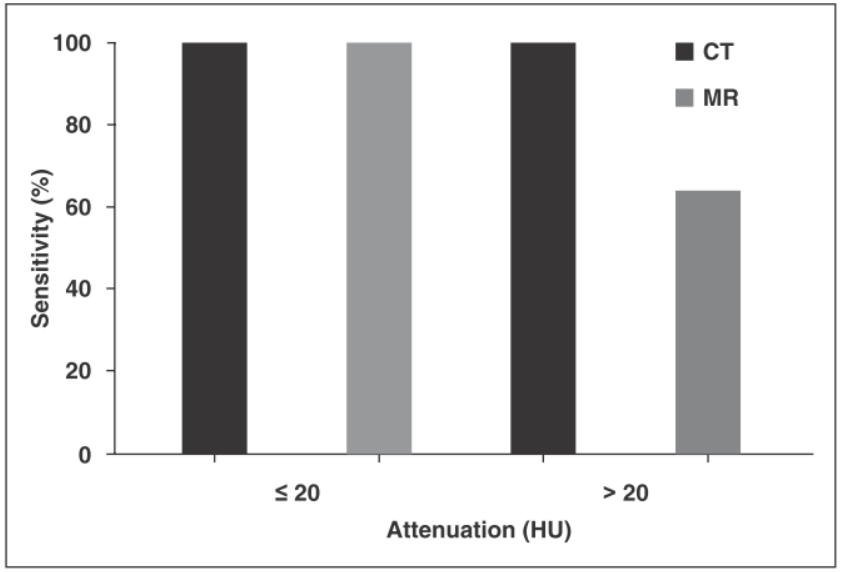

Fig. 5—Graph shows CT and MRI sensitivities for lipid-poor adenomas measuring 20 HU or less on unenhanced CT are both 100% (12/12), whereas those for lipid-poor adenomas measuring greater than 20 HU are 100% (25/25) and 64.0% (16/25), respectively.

Histopathologic confirmation in few cases

European Journal of Radiology 65 (2008) 154–162

Nagihan Inan*, Arzu Arslan, Gur Akansel, Yonca Anik, N. Cem Balci, Ali Demirci

Table 2
Quantitative analysis of the dynamic contrast enhanced MR images

	Adenomas ($n=48$)	Malignant masses ($n=16$)	p
SI			
0th second	823.62 ± 188.1	746.12 ± 156.03	0.078
25th second	1273.42 ± 345.81	1073.99 ± 261.66	0.010
50th second	1314.58 ± 288.58	1220.91 ± 328	0.117
75th second	1260.11 ± 299.9	1219.75 ± 324.3	0.394
100th second	1177.73 ± 283.74	1135.73 ± 328.55	0.402
Time-to-peak enhancement (s)	40.8 ± 17.03	65.55 ± 10.79	0.000
Wash-in-rate	19.61 ± 8.85	13.63 ± 7.06	0.011
$Wo_{max/100\,s}$	0.17 ± 0.11	0.12 ± 0.11	0.121
Maximum relative enhancement (%)	62.75 ± 30.78	63.16 ± 33.1	0.687

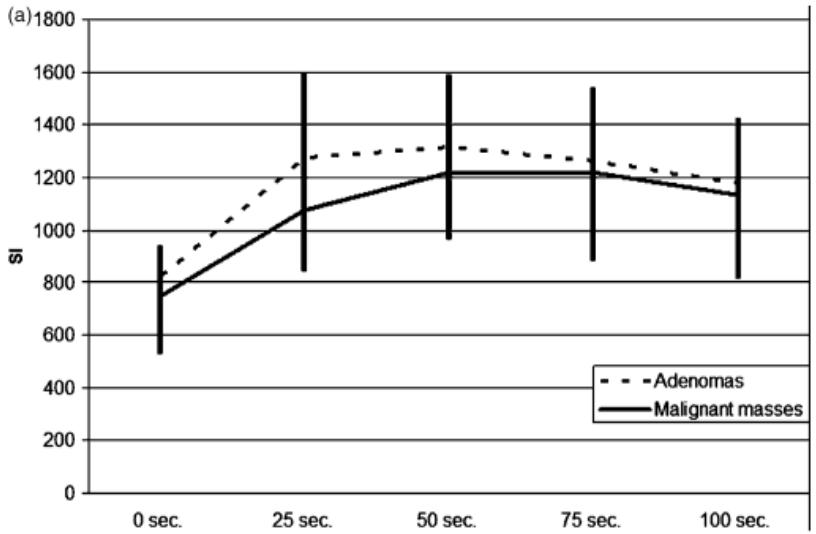

Dynamic contrast enhanced MRI in the differential diagnosis of adrenal adenomas and malignant adrenal masses

European Journal of Radiology 65 (2008) 154–162

Nagihan Inan*, Arzu Arslan, Gur Akansel, Yonca Anik, N. Cem Balci, Ali Demirci

With a cut-off value of 52.85 s, the time-to-peak enhancement had 87.5% sensitivity and 80% specificity.

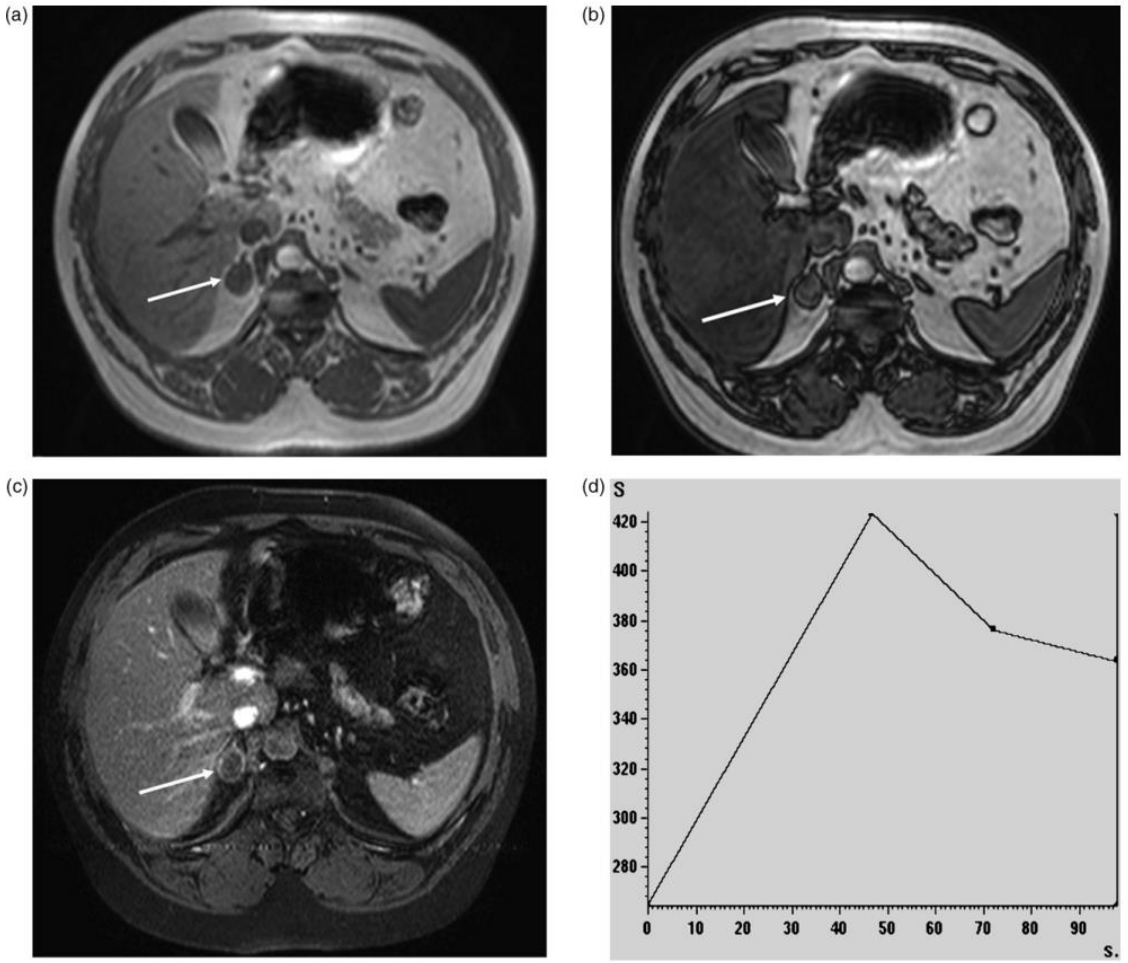

The malignant masses:
13 metastases
2 adrenocortical carcinomas
1 neuroblastoma

Fig. 2. Forty-seven-year-old woman with an atypical adenoma. Lesion was unchanged during 12-months of follow-up. (a) In-phase and (b) out-of-phase images. There is no remarkable signal loss in the out-of-phase image. (c) Postcontrast 5th minute fat suppressed T1-weighted image. Note the peripheral ring-shaped enhancement (arrow). (d) SI–time curve and (e) quantitative interpretation of the curve, automatically calculated by the workstation. Time-to-peak enhancement less than 52 s (46.7 s) implies atypical adenoma.

Figure 6. Drawing shows an adrenocortical carcinoma.

Arq Bras Endocrinol Metab 2007;51/8

ANJU SAHDEV
RODNEY H. REZNEK
JANE EVANSON
ASHLEY B. GROSSMAN

Adrenal carcinoma

al tumours are more common in adults (23). In adults, 30–40% of adrenal carcinomas are hyperfunctioning. Hypercortisolism and virilisation are the most common endocrine manifestations although trace amounts of other hormones may be produced. In our series, carcinomas accounted for 27% of ACTH-independent Cushing's syndrome (24) (figure 9).

CT typically shows a unilateral mass, usually over 6 cm in size with an inhomogeneous appearance due to necrosis, haemorrhage, fibrosis and calcification. Smaller carcinomas may resemble adenomas. Recent studies combining non-enhanced, delayed-enhancement CT attenuation and percentage of contrast enhancement washout attenuation values at 10 minutes showed adrenal carcinomas all behaved as non-adenomas. Using these criteria adenomas were distinguished from adrenal carcinomas and phaeochromocytomas with a sensitivity and specificity of 100% (28,29). As with renal tumours, careful assessment of the draining venous structures is essential on imaging together with identification of direct infiltration of adjacent viscera such as the liver, kidney or spleen. Venous invasion occurred in 40% of our series (23). Multiplanar imaging using MRI or multidetector CT allows better assessment of invasion into adjacent structures, important for surgical planning. Metastases to the liver and lungs are not infrequent. A large mass, high suspicion of malignancy and surrounding invasion preclude laproscopic adrenalectomy or even biopsy, which may be suitable for small unilateral benign adenomas.

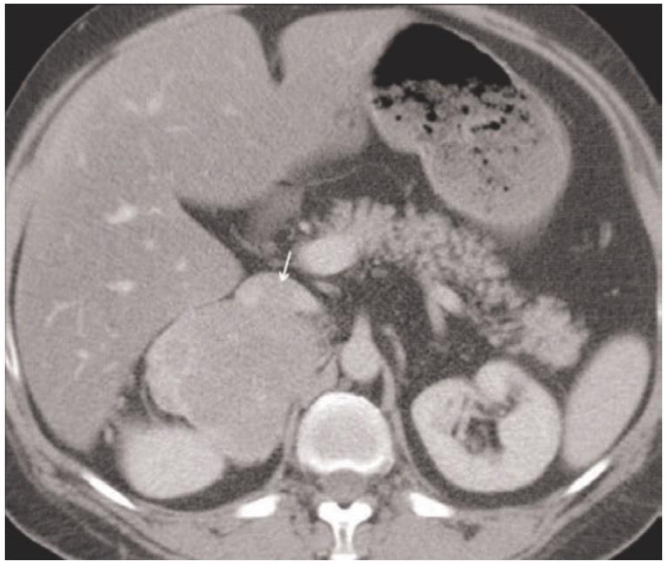

Figure 9. Adrenal carcinoma on CT scanning. Post-contrast CT of the adrenal glands acquired 60 seconds after intravenous contrast administration showing a large heterogeneous right adrenal mass in a patient with ACTH-independent Cushing's disease. There is direct invasion of the adjacent inferior vena cava (arrow). The appearances are typical for adrenal carcinoma and this was confirmed histologically.

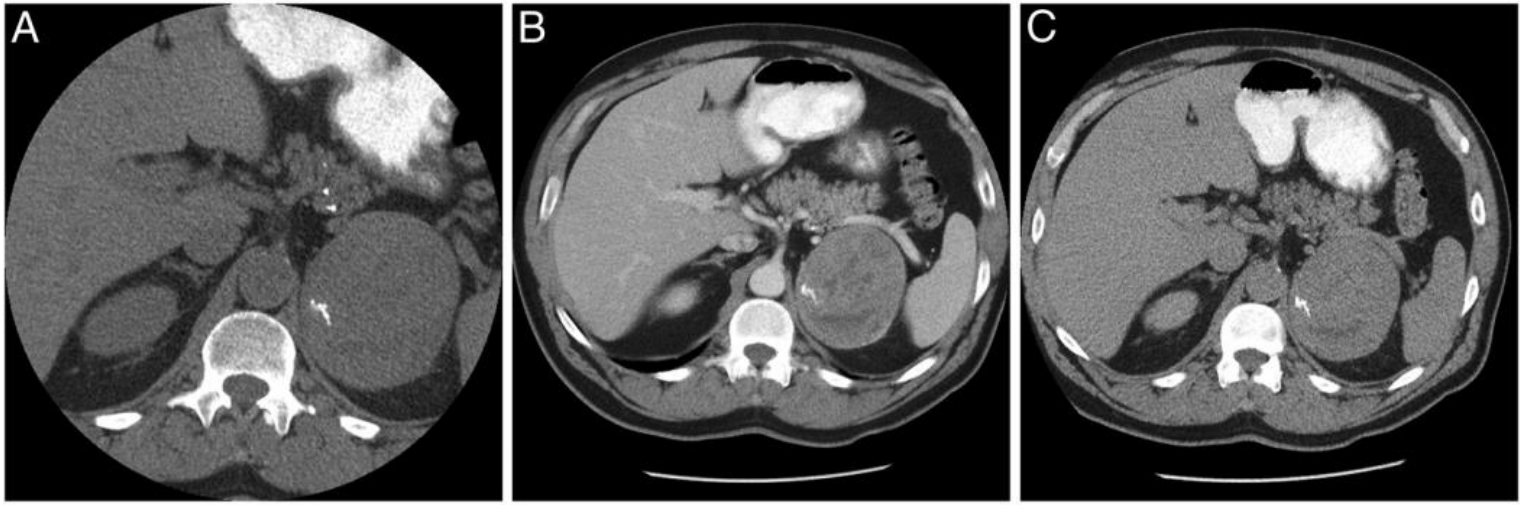

Figure 3. ACC. A, Precontrast fairly homogeneous with calcification (30 HU). B, Early-phase contrast with heterogeneous enhancement. C, Delayed phase (15 minutes).

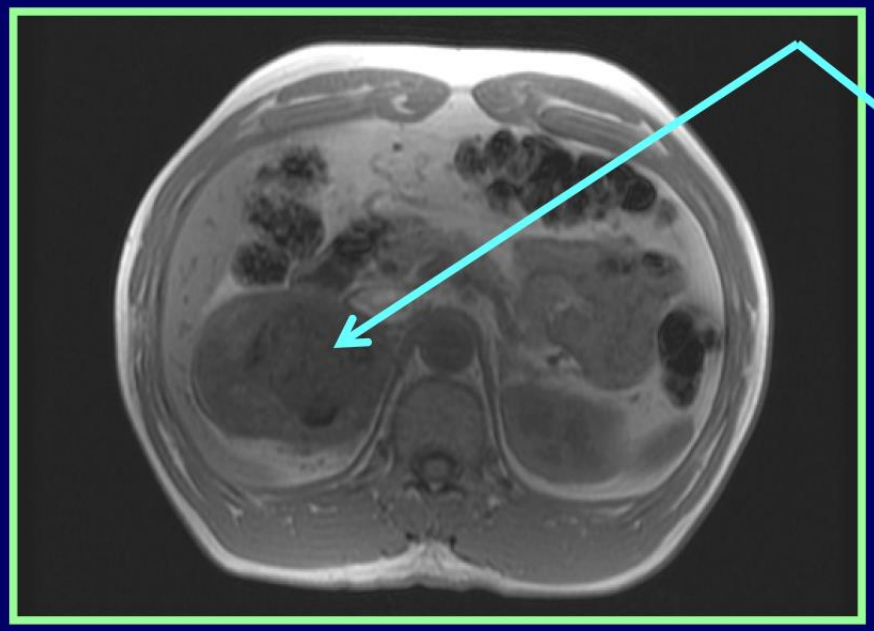

T1-Weighted axial image of abdomen, in-phase

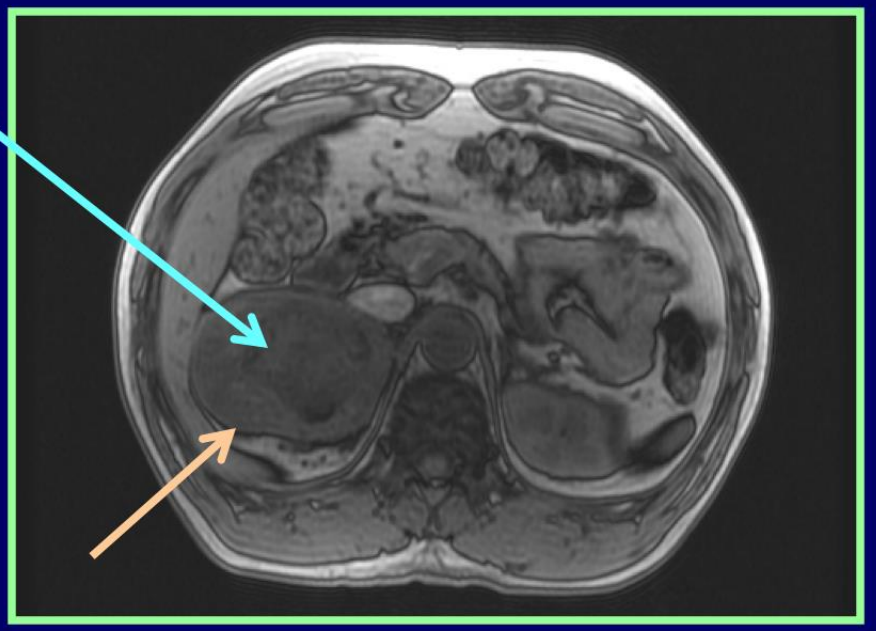

T1-Weighted axial image of abdomen, out-of-phase

- No change in signal intensity between in/out-of-phase images.
- No India Ink artifact within mass. (Seen between mass and fat plane in out-of-phase).

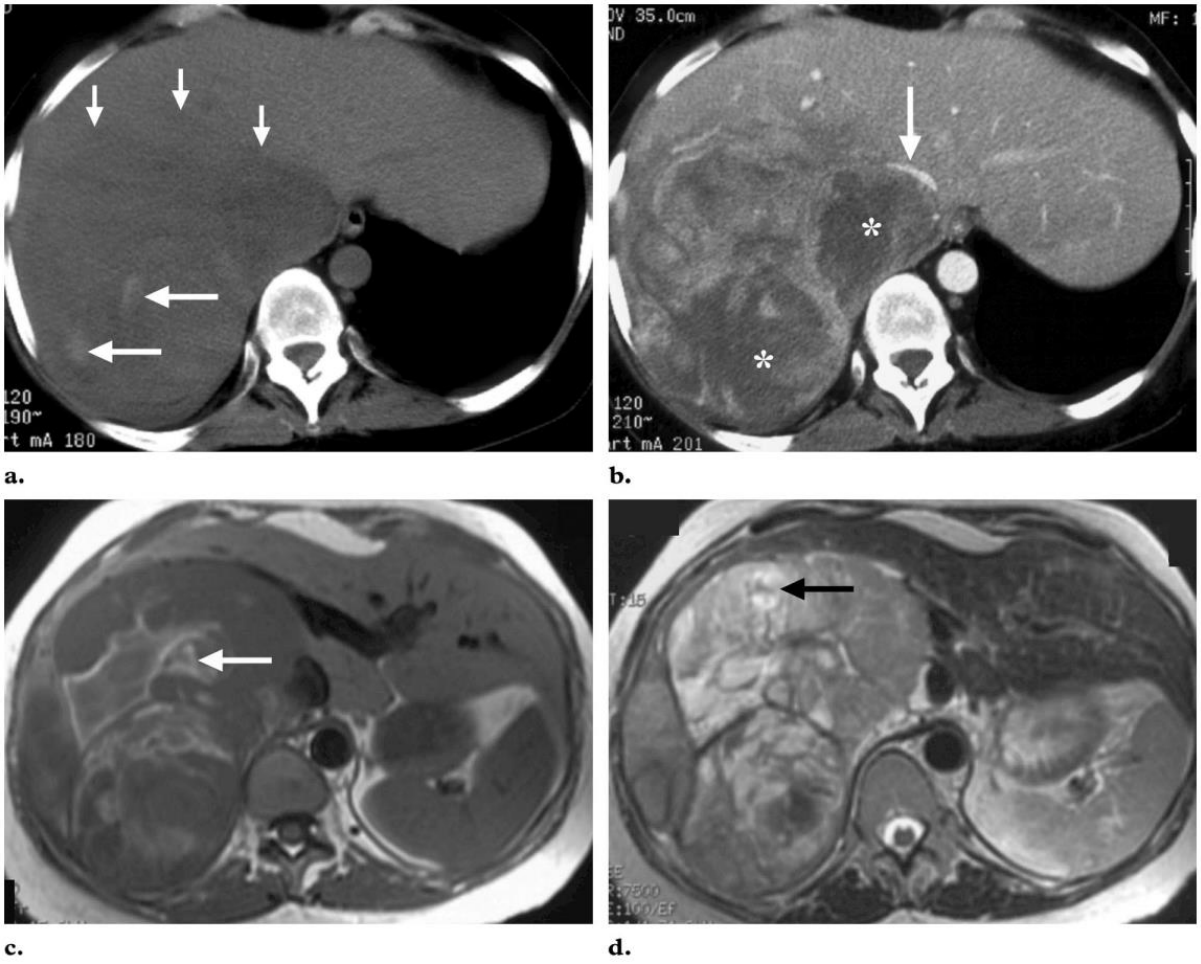

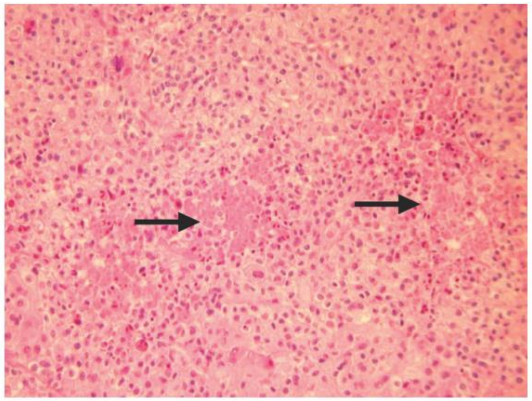

Figure 6. Adrenal carcinoma in a 32-year-old woman with Cushing syndrome. **(a)** Unenhanced CT scan demonstrates a large, low-attenuation suprarenal mass (short arrows) containing areas of high attenuation (long arrows) that are consistent with hemorrhage. **(b)** Contrast-enhanced CT scan demonstrates the mass with heterogeneous enhancement. Large areas of necrosis are also seen (*). Note the anterior displacement and compression of the inferior vena cava (IVC) (arrow). **(c)** Axial T1-weighted MR image (500/14) demonstrates high-signal-intensity areas within the mass (arrow), a finding that is consistent with hemorrhage. **(d)** Axial fast spin-echo T2-weighted MR image (7,500/100) also demonstrates extensive high-signal-intensity areas within the mass (arrow), a finding that is consistent with necrosis. **(e)** Photomicrograph (original magnification, ×100; H-E stain) demonstrates amorphous necrosis (arrows), a finding that is seen in the majority of adrenal carcinomas.

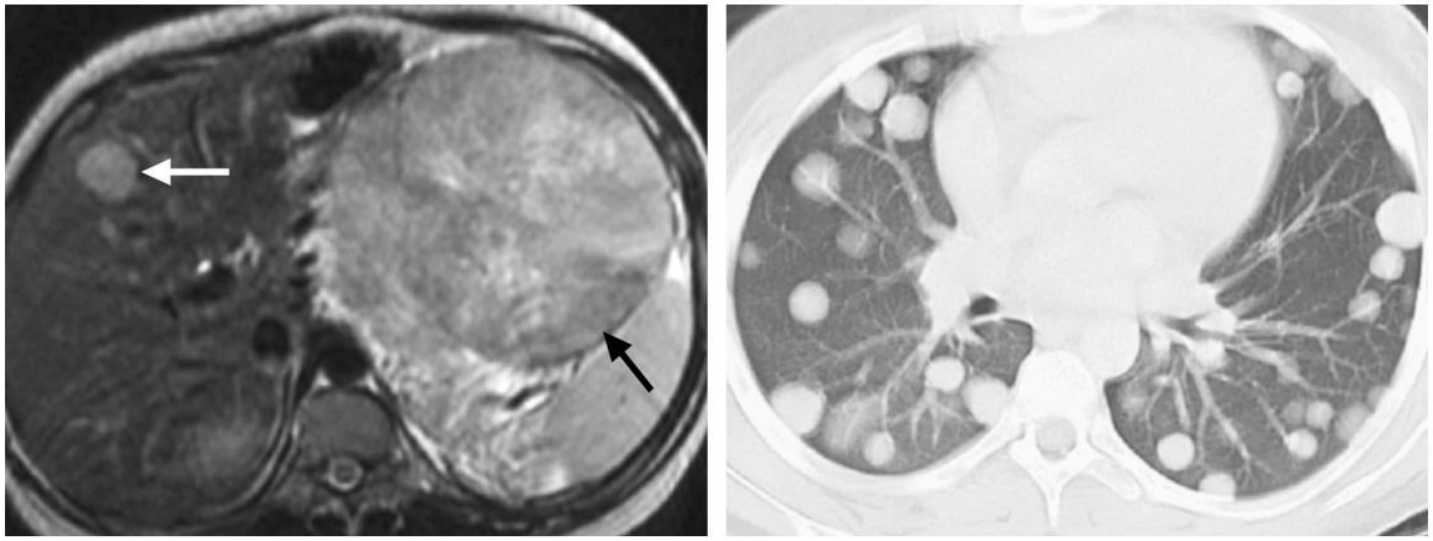

a. b.

Figure 7. Adrenal carcinoma in an 11-year-old girl with Cushing syndrome and virilization. **(a)** Axial fast spin-echo T2-weighted MR image (5,000/105) shows a large, left-sided adrenocortical carcinoma (black arrow) and a liver metastasis (white arrow). **(b)** Chest CT scan shows extensive lung metastases.

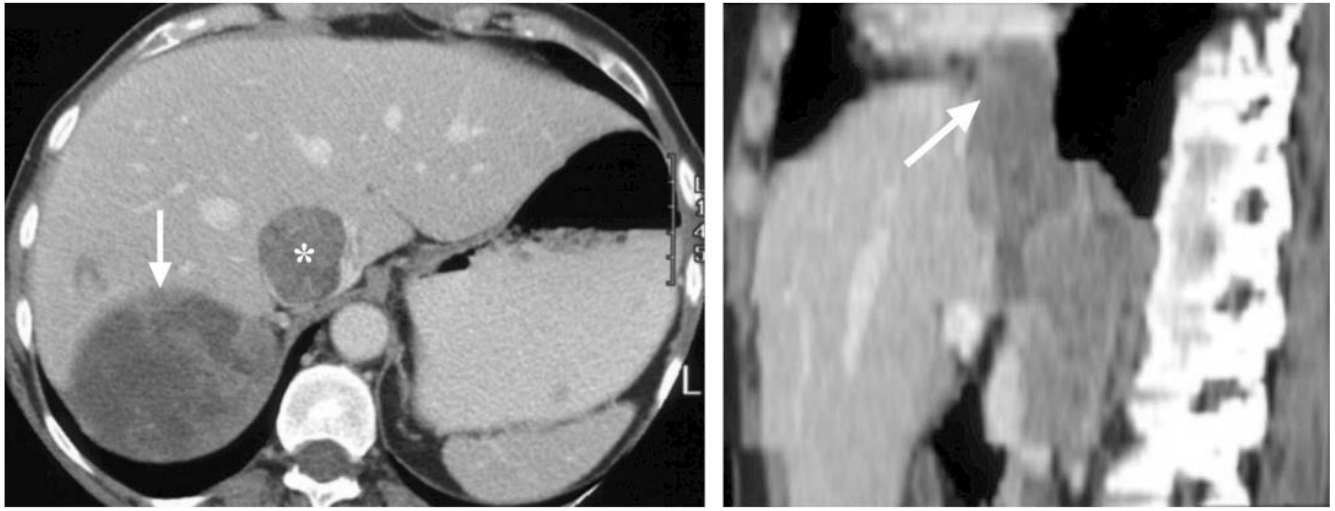

a. b.

Figure 8. Adrenocortical carcinoma in a 45-year-old woman with a history of hypertension. **(a)** Contrast-enhanced CT scan demonstrates a large, heterogeneously enhancing mass in the right suprarenal region (arrow) with extension into the IVC (*). **(b)** Sagittal thin-section reformatted image elegantly demonstrates tumor extension into the IVC and right atrium (arrow).

Adrenal masses: the value of additional fluorodeoxyglucose-positron emission tomography/computed tomography (FDG-PET/CT) in differentiating between benign and malignant lesions

Ann Nucl Med (2009) 23:349–354

Masahiro Okada · Taro Shimono · Yoshihiro Komeya · Rina Ando · Yuki Kagawa · Takashi Katsube · Masatomo Kuwabara · Yukinobu Yagyu · Seishi Kumano · Izumi Imaoka · Norio Tsuchiya · Ryuichiro Ashikaga · Makoto Hosono · Takamichi Murakami

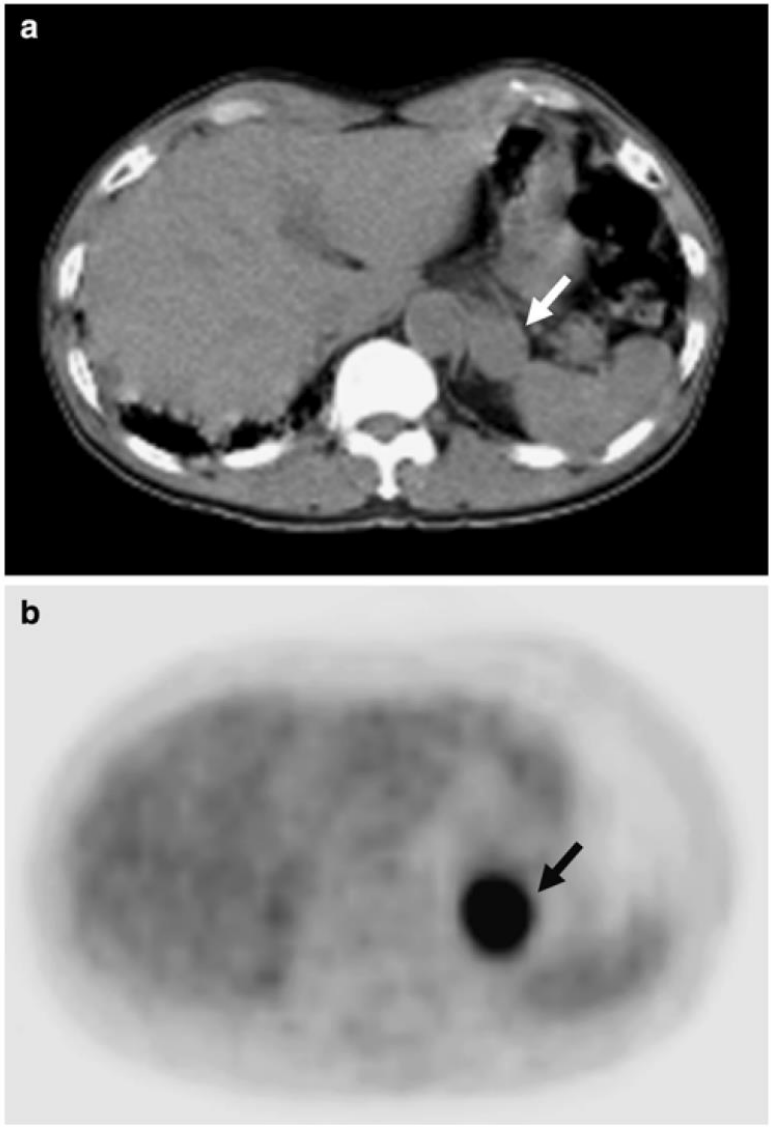

Fig. 1 Integrated FDG-PET/CT of a patient with adrenal malignant lesion. The PET and computed tomography (CT) images are presented separately. **a** Unenhanced CT obtained from integrated PET/CT. The *arrow* indicates a 27-mm left adrenal tumor with CT attenuation value of 24 HU. **b** PET image obtained from integrated PET/CT. The *arrow* indicates a left adrenal tumor with higher uptake (SUV_{max}, 12.6) than that of liver parenchyma

^{18}F-Fluorodeoxyglucose Positron Emission Tomography for the Diagnosis of Adrenocortical Tumors: A Prospective Study in 77 Operated Patients

J Clin Endocrinol Metab, May 2009, 94(5):1713–1722

Lionel Groussin, Gérald Bonardel, Stéphane Silvéra, Frédérique Tissier, Joël Coste, Gwenaelle Abiven, Rossella Libé, Marie Bienvenu, Jean-Louis Alberini, Sylvie Salenave, Philippe Bouchard, Jérôme Bertherat, Bertrand Dousset, Paul Legmann, Bruno Richard, Hervé Foehrenbach, Xavier Bertagna, and Florence Tenenbaum

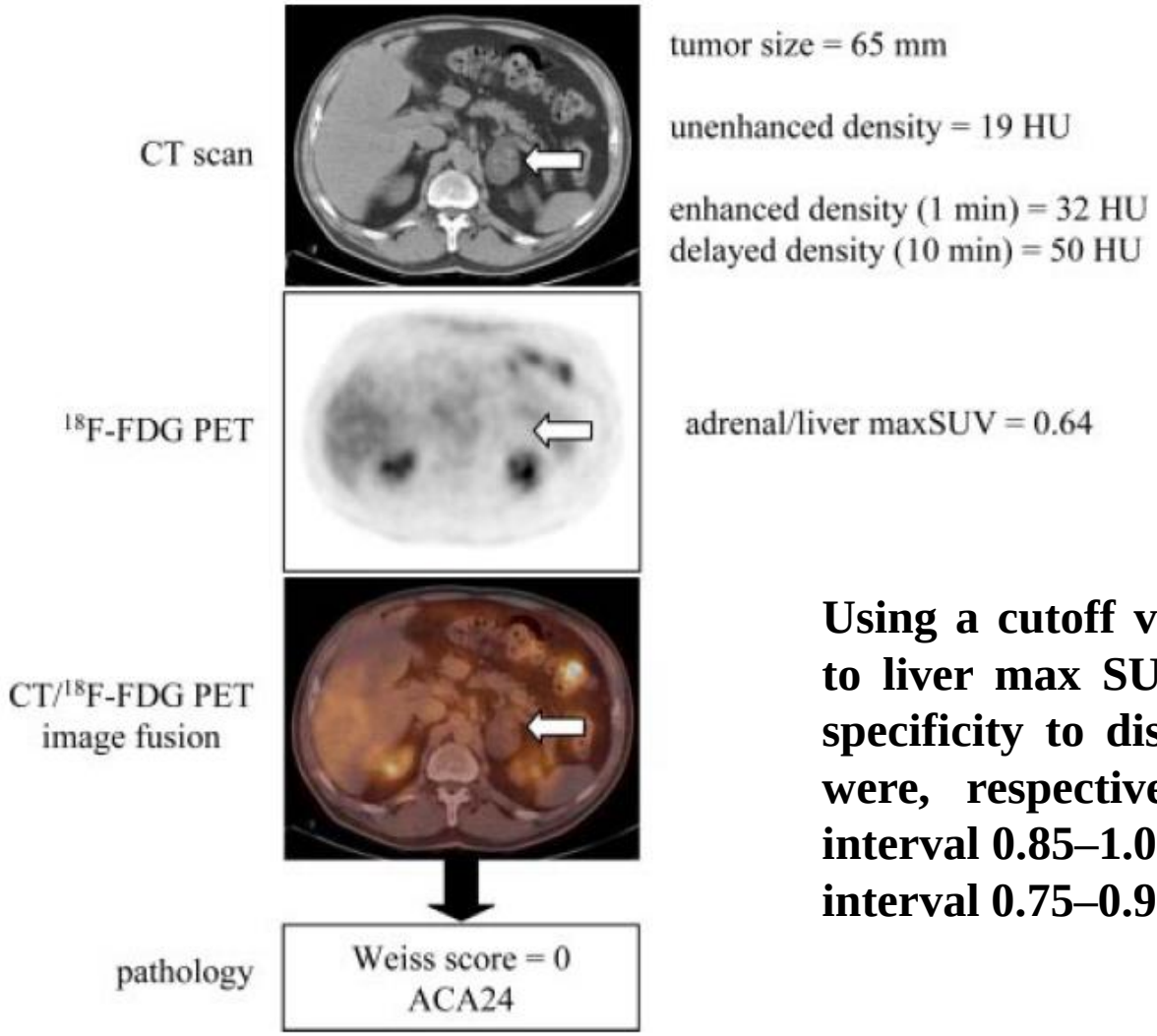

Using a cutoff value above 1.45 for adrenal to liver max SUV ratio, the sensitivity and specificity to distinguish ACAs from ACCs were, respectively, 1.00 (95% confidence interval 0.85–1.00) and 0.88 (95% confidence interval 0.75–0.96).

FIG. 5. ^{18}F-FDG predicts benignity of adrenal incindentalomas.

Endocrine Reviews, April 2014, 35(2):282–326

Adrenocortical Carcinoma

Tobias Else, Alex C. Kim, Aaron Sabolch, Victoria M. Raymond, Asha Kandathil, Elaine M. Caoili, Shruti Jolly, Barbra S. Miller, Thomas J. Giordano, and Gary D. Hammer

Table 4. Imaging Characteristics of ACC

Lesion Characteristics	ACC	ACA
Size	>4 cm	<4 cm
Necrosis	+	−
Hemorrhage	+	−
Calcification	+/−	−
CT density	Heterogeneous, >10 HU	Homogeneous, <10 HU
Chemical-shift MRI	Heterogeneous signal drop +/−	Homogeneous signal drop
Contrast enhancement	Heterogeneous, absolute % washout <60%	Homogeneous, absolute % washout >60%
SUV on [^{18}F]FDG-PET/CT	Adrenal to liver SUV ratio >1.45	Adrenal to liver SUV ratio <1.45

Clinicopathological correlates of adrenal Cushing's syndrome

J Clin Pathol 2015;**68**:175–186.

Kai Duan,[1,2] Karen Gomez Hernandez,[3,4] Ozgur Mete[1,2,4]

Table 2 Clinical, biochemical and radiological features of adrenal Cushing

			Primary adrenocortical hyperplasia			
			Macronodular hyperplasia		Micronodular hyperplasia	
	Adrenocortical adenoma	**Adrenocortical carcinoma**	**BMAH**	**c-BMAH**	**PPNAD**	**MAD**
Frequency	~55%	~35%	Estimated 10%			
Age	All ages	All ages; familial cases in childhood	Fifth to sixth decade	Early childhood	Childhood or early adulthood	
Clinical presentation	Mild-to-severe Cushing	Moderate-to-severe Cushing with rapid onset and possible virilisation	Mild Cushing with insidious onset	Moderate-to-severe Cushing	Moderate-to-severe Cushing	
Biochemical features	Negative Liddle's test	Negative Liddle's test	Negative Liddle's test	Negative Liddle's test	Paradoxical cortisol response in Liddle's test	Negative Liddle's test
Radiological features	Solitary mass, often <4 cm, defined margins, homogeneous, <10 HFU, absolute washout >60%	Solitary mass, often >4 cm, irregular margins, heterogenous, >10 HFU, absolute washout <60%	Marked bilateral adrenal enlargement with multiple large non-pigmented nodules (1–5 cm)		Normal or small size adrenal glands with occasional small nodules (<1 cm)	

BMAH, primary bilateral macronodular adrenocortical hyperplasia; c-BMAH, childhood BMAH; HFU, Hounsfield unit; MAD, non-pigmented micronodular adrenocortical disease; PPNAD, primary pigmented nodular adrenocortical disease.

Primary pigmented nodular adrenocortical disease (PPNAD)

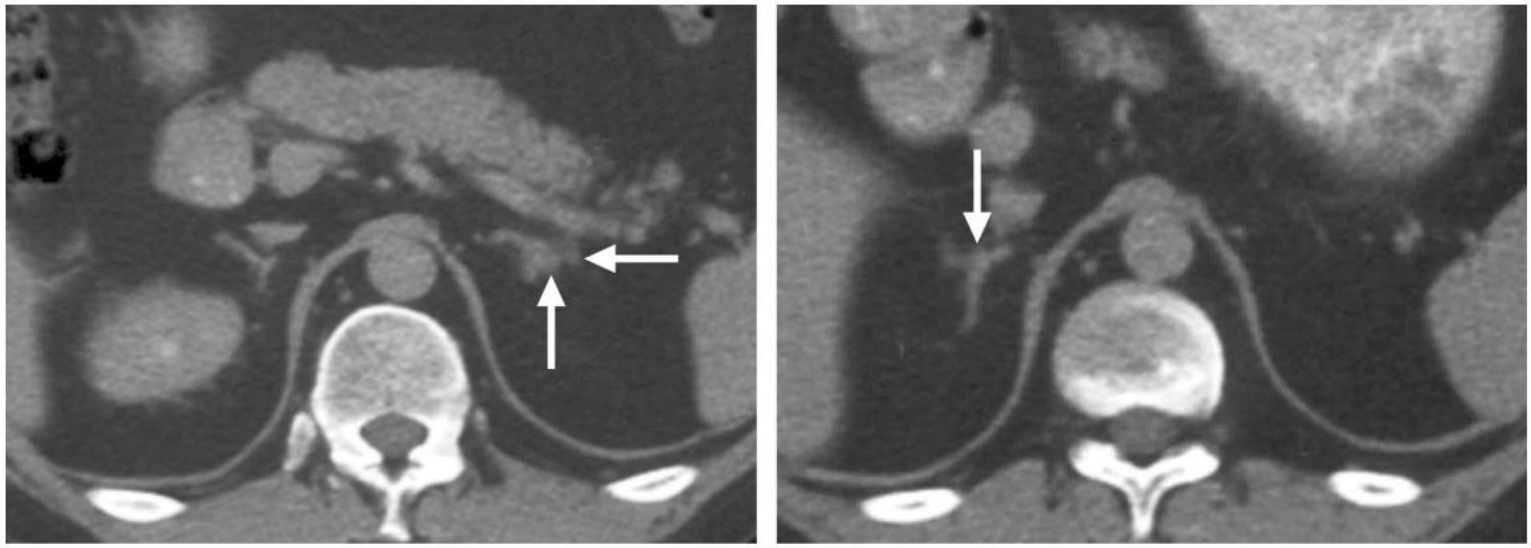

a. b.

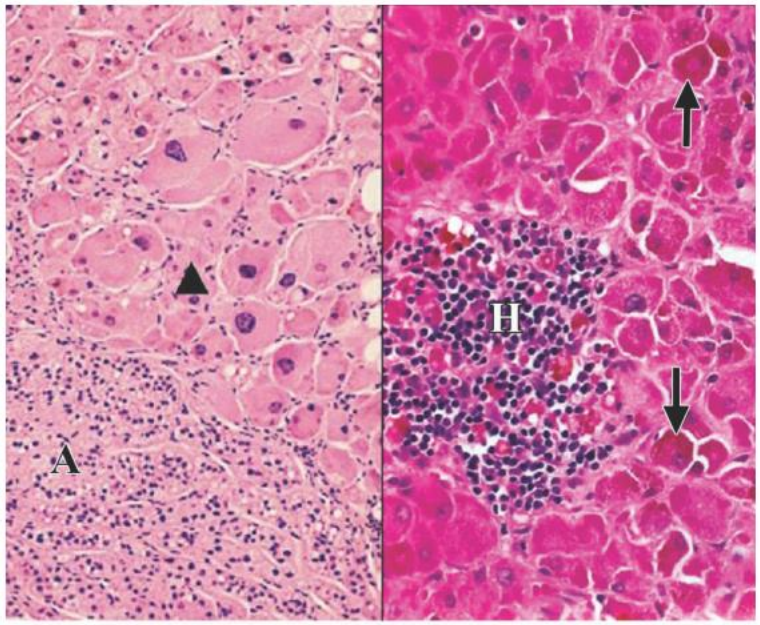

c.

Figure 9. PPNAD in a 28-year-old man. **(a, b)** Delayed contrast-enhanced CT scans show small nodules in the left **(a)** and right **(b)** adrenal glands (arrows). The remaining portions of the glands do not appear hyperplastic. **(c)** Photomicrograph (original magnification, ×200; H-E stain) (left) shows nodules of enlarged and hyperchromatic cells (hyperplastic adrenocortical cells) (arrowhead) alternating with normal adrenocortical parenchyma *(A)*. Photomicrograph (original magnification, ×200; H-E stain) (right) reveals deeply eosinophilic cells with an abundance of lipofuscin pigment (arrows) and a focal cluster of hyperchromatic cells with dark blue staining *(H)*. The latter are hematopoietic cells and are commonly seen incidentally in normal adrenal tissue. These findings indicate the presence of PPNAD, also known as micronodular hyperplasia.

CT Findings of Primary Pigmented Nodular Adrenocortical Disease: Rare Cause of ACTH-Independent Cushing Syndrome

Nikos Courcoutsakis
Eunice Kennedy Shriver, National Institute of Child Health and Human Development National Institutes of Health Bethesda, MD
Democritus University of Thrace Alexandroupolis, Greece
Panos Prassopoulos
Democritus University of Thrace Alexandroupolis, Greece
Constantine A. Stratakis
Eunice Kennedy Shriver, National Institute of Child Health and Human Development National Institutes of Health Bethesda, MD

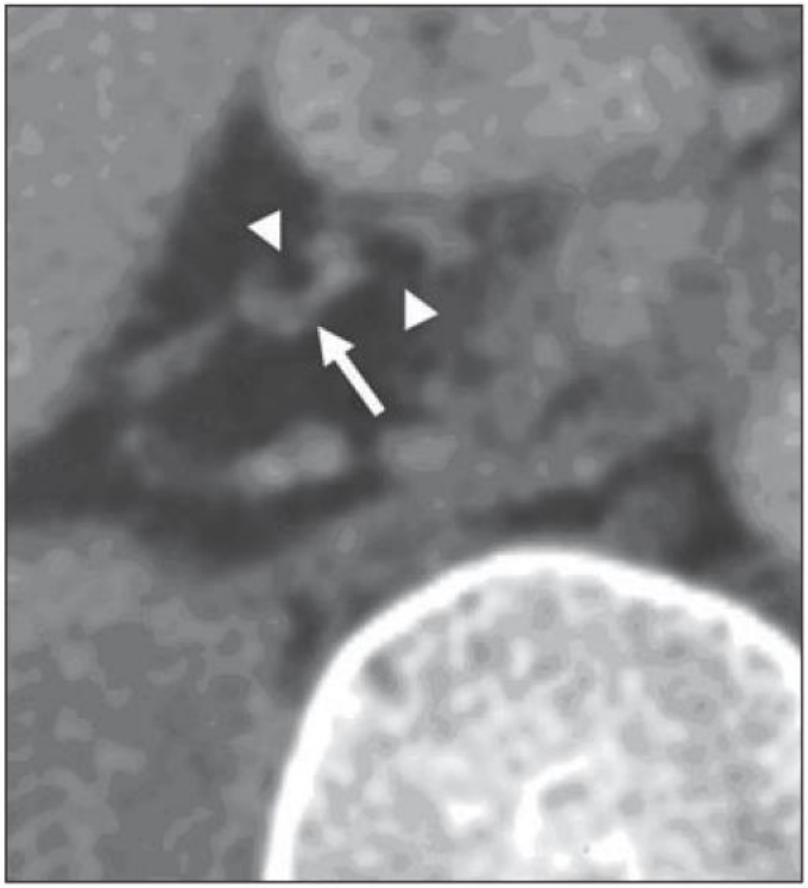

Fig. 1—Axial enhanced CT image of right adrenal gland of 19-year-old man with Cushing syndrome due to primary pigmented nodular adrenocortical disease shows atrophic gland with characteristic nodule (*arrow*) and hypodense pigments (*arrowheads*).

Imaging in Cushing's Syndrome

Arq Bras Endocrinol Metab 2007;51/8

Anju Sahdev
Rodney H. Reznek
Jane Evanson
Ashley B. Grossman

ACTH-independent macronodular adrenal hyperplasia (AIMAH)

ogy of AIMAH remains obscure. The imaging appearances of the adrenal glands are striking. They show massive bilateral adrenal enlargement, nodularity and distortion of adrenal contour. Nodules vary in size from 1 cm to 5.5 cm and on CT are of low attenuation in keeping with lipid rich adenomas (figure 10). Coronal imaging, either with MDCT

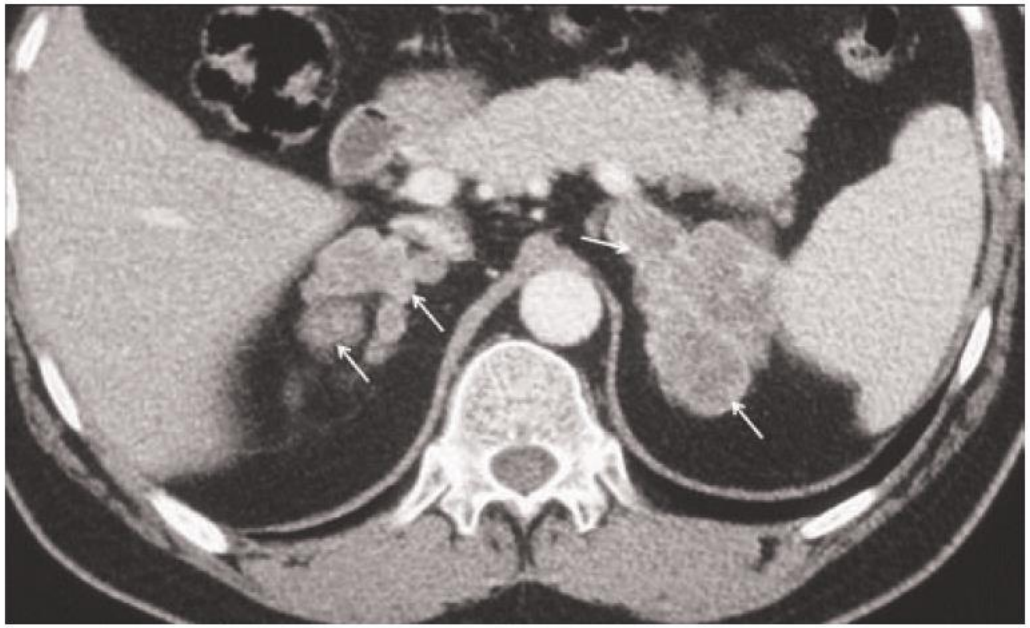

Figure 10. ACTH-independent massive adrenal hyperplasia. Post-contrast CT of the adrenal glands acquired 60 seconds after intravenous contrast administration demonstrating massive nodular hyperplasia of both adrenal glands (arrows). The suppressed ACTH levels distinguish this macronodular hyperplasia from the ACTH-dependent hyperplasia in pituitary adenomas and ectopic ACTH production.

ACTH-independent macronodular adrenal hyperplasia (AIMAH)

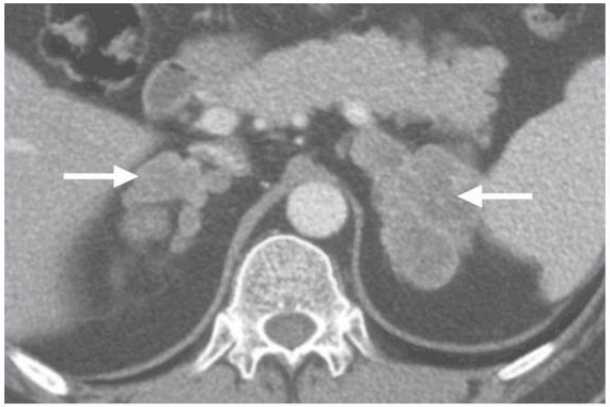

a.

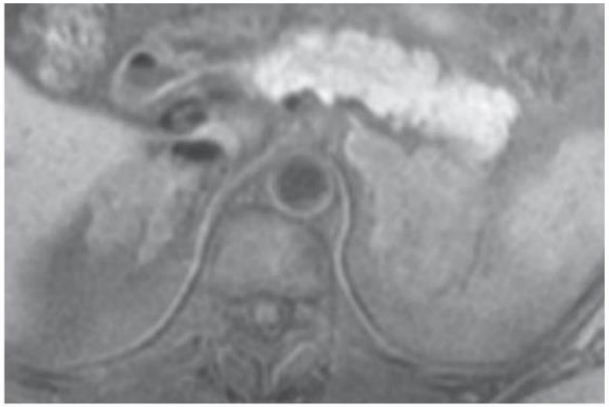

b.

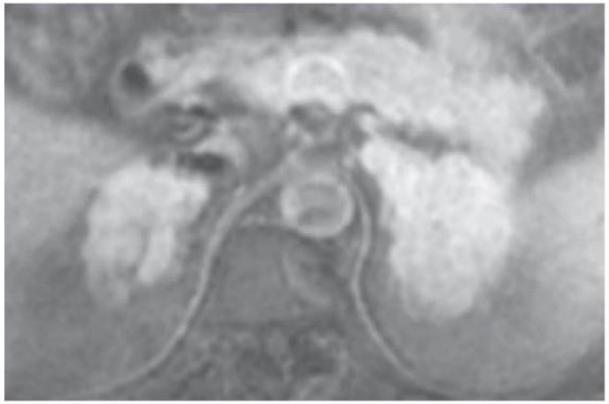

c.

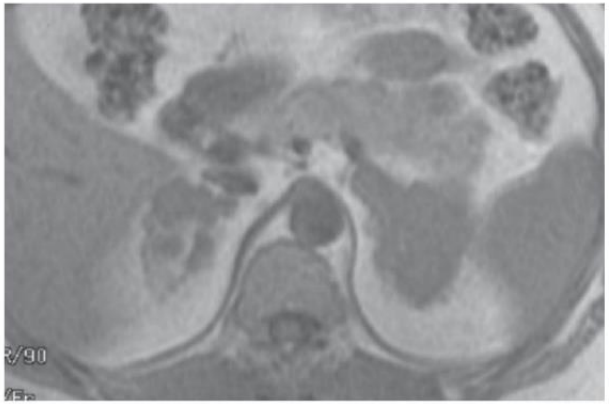

d.

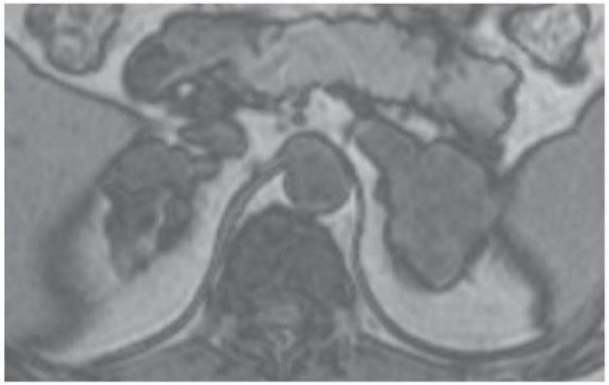

e.

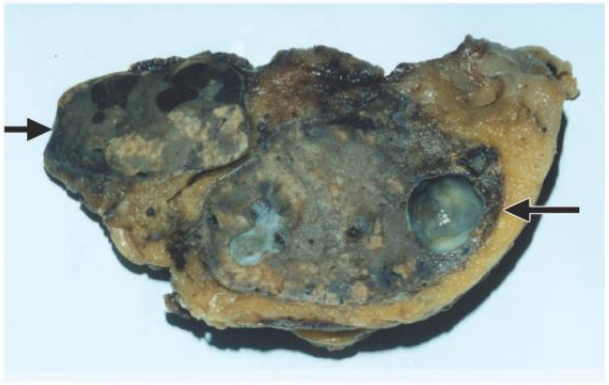

f.

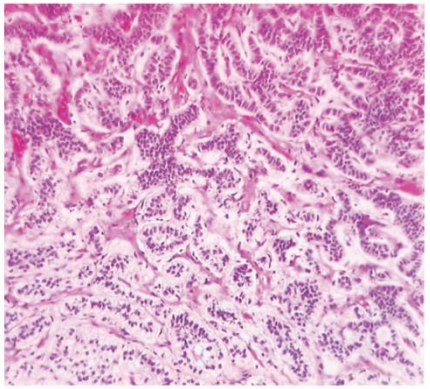

g.

Figure 10. AIMAH in a 50-year-old man with Cushing syndrome. **(a)** Contrast-enhanced CT scan shows massive hyperplasia of both adrenal glands (arrows), which still retain their adreniform contour. **(b, c)** Axial unenhanced **(b)** and contrast-enhanced **(c)** fat-saturated spin-echo T1-weighted MR images (500/16) show intense homogeneous enhancement of the hyperplastic nodular glands. **(d, e)** Axial in-phase (150/4.2) **(d)** and out-of-phase (150/2.3) **(e)** FMPSPGR T1-weighted MR images (flip angle = 90°) demonstrate 42% signal dropout within the glands with the out-of-phase sequence, a finding that indicates the presence of intracellular lipid. **(f)** Sectioned gross resected specimen of the left adrenal gland shows marked cortical expansion with multiple nodules (arrows). **(g)** Photomicrograph (original magnification, ×200; H-E stain) reveals sheets of largely fascicular zone cells and areas of glomerular zone cells, which have a more compact trabecular pattern. No malignant or pigmented cells are seen.

Adrenocorticotropin-independent Macronodular Adrenal Hyperplasia: An Uncommon Cause of Primary Adrenal Hypercortisolism[1]

John L. Doppman, MD
George P. Chrousos, MD
Dimitris A. Papanicolaou, MD
Constantine A. Stratakis, MD, DSc
H. Richard Alexander, MD
Lynnette K. Nieman, MD

Radiology · September 2000

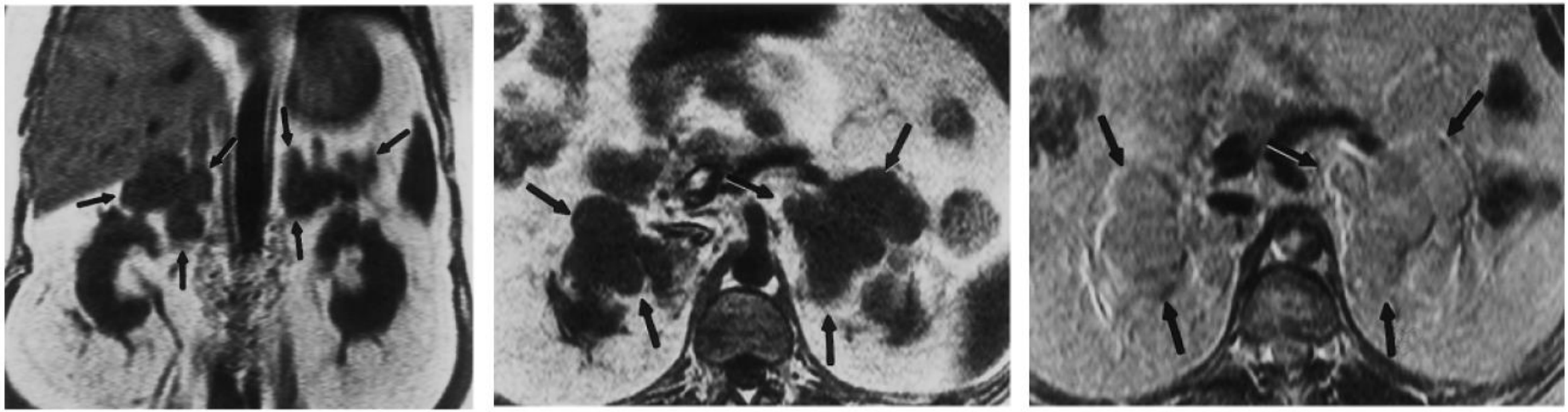

a. b. c.

Figure 2. Patient 10. **(a)** The extent of adrenal enlargement (arrows) is well demonstrated on this coronal T1-weighted (300/10) spin-echo MR image. **(b, c)** Macronodular hyperplastic adrenal glands (arrows) are **(b)** hypointense relative to the liver on a transverse T1-weighted (300/10) spin-echo MR image and **(c)** minimally hyperintense on a transverse T2-weighted (2,000/80) spin-echo MR image.

On MRI, T1-weighted images are *hypointense* relative to the liver and isointense relative to muscle. T2-weighted images tend to be *hyperintense* relative to the liver.

In contrast, the nodules of patients with chronic ACTH stimulation appear *isointense* relative to the liver on T2-weighted MR images.

Semin Nucl Med 36:212-227 © 2006

Anca M. Avram, MD,* Lorraine M. Fig, MBChB, MPH,*,† and Milton D. Gross, MD*,†

Seminars in NUCLEAR MEDICINE

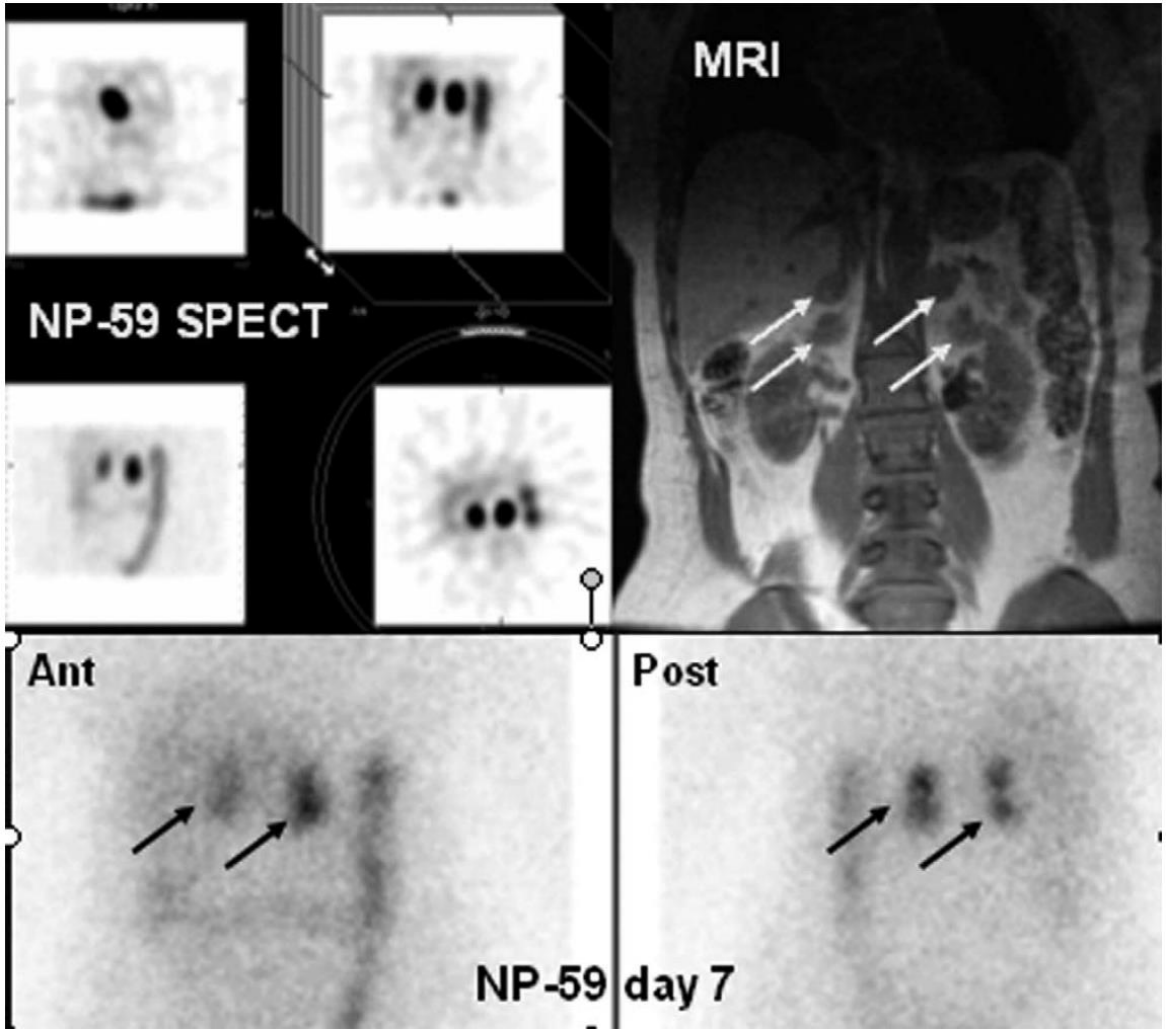

Figure 4 NP-59 scan (SPECT and planar images) demonstrating bilateral macronodular adrenal hyperplasia in a 60-year-old woman presenting with bilateral nodular enlargement of the adrenals on cross-sectional anatomic imaging and biochemical evidence of ACTH-independent Cushing syndrome. MRI demonstrates 2 nodular masses involving each adrenal gland.

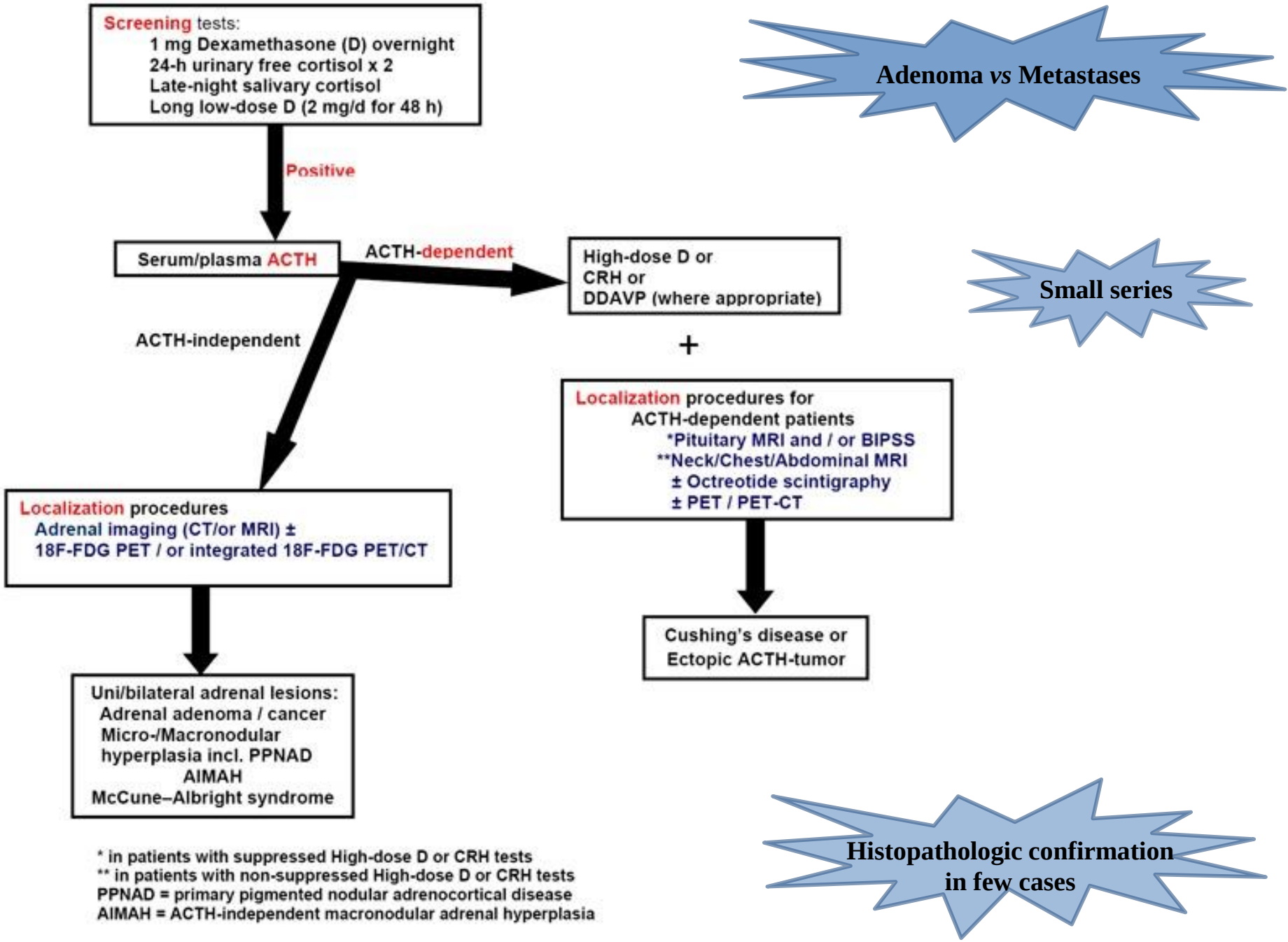
Screening tests:
1 mg Dexamethasone (D) overnight
24-h urinary free cortisol x 2
Late-night salivary cortisol
Long low-dose D (2 mg/d for 48 h)
Positive
Serum/plasma ACTH
ACTH-dependent
High-dose D or
CRH or
DDAVP (where appropriate)
+
ACTH-independent
Localization procedures for
ACTH-dependent patients
*Pituitary MRI and / or BIPSS
**Neck/Chest/Abdominal MRI
± Octreotide scintigraphy
± PET / PET-CT
Localization procedures
Adrenal imaging (CT/or MRI) ±
18F-FDG PET / or integrated 18F-FDG PET/CT
Cushing's disease or
Ectopic ACTH-tumor
Uni/bilateral adrenal lesions:
Adrenal adenoma / cancer
Micro-/Macronodular
hyperplasia incl. PPNAD
AIMAH
McCune–Albright syndrome
* in patients with suppressed High-dose D or CRH tests
** in patients with non-suppressed High-dose D or CRH tests
PPNAD = primary pigmented nodular adrenocortical disease
AIMAH = ACTH-independent macronodular adrenal hyperplasia
Adenoma vs Metastases
Small series
Histopathologic confirmation
in few cases

Thank you for your attention